The 2009 IEEE/RSJ International Conference on
Intelligent Robots and Systems
October 11-15, 2009 St. Louis, USA

Analytical and Computational Modeling of Robotic Fish Propelled by Soft Actuation Material-based Active Joints

Mart Anton, Zheng Chen, Maarja Kruusmaa and Xiaobo Tan

Abstract— **Soft actuation materials, such as Ionic Polymer-Metal Composites (IPMCs), are gaining increasing interest in robotic applications since they lead to compact and biomimetic designs. In this paper, we propose the use of soft actuation materials as active joints for propelling biomimetic robotic fish. An analytical model is developed to compute the thrust force generated by a two-link tail and the resulting moments in the active joints. The computed joint moments can be combined with internal dynamics of actuation materials to provide realistic kinematic constraints for the joints. Computational fluid dynamics (CFD) modeling is also adopted to examine the flow field, the produced thrust, and the bending moments in joints for the two-link tail. Good agreement is achieved between the analytical modeling and the CFD modeling, which points to a promising two-tier framework for the understanding and optimization of robotic fish with a multi-link tail. We also show that, comparing to a one-link bending tail, a two-link tail is able to produce much higher thrust and more versatile maneuvers, such as backward swimming.**

I. Introduction

Inspired by the speed, efficiency, and maneuverability of real fish [1] and driven by the desire to mimic such capabilities, researchers have studied extensively the use of oscillating or undulating foils or body for propelling underwater vehicles or robots. A number of prototypes of robotic fish have been reported over the past decade (see, e.g., [2]–[7], some of which have demonstrated untethered or even autonomous swimming in controlled environments (tanks or pools). While the existing work on biomimetic propulsion has been predominantly focused on rigid, oscillating plates or foils driven by motors [4], [7], robotic fish using emerging soft actuation materials are gaining increasing interest. Electroactive polymers (EAP's), also known as artificial muscles, are attractive for aquatic robots because they are flexible and produce significant bending deformations under low voltages (several volts) [8], [9]. Without using motors and the associated complex transmission systems, soft actuation material-enabled robotic fish could achieve compact and biomimetic design. Two particularly promising classes of EAP materials are ionic polymer-metal composites (IPMC's) [8] and conjugated polymers [10], [11]. IPMC-based swimming robots have been reported by several groups (e.g., [3], [5], [6], [12]–[15]). Most of these robots use the bending of (relatively long) individual IPMC beams to produce propulsion and maneuvering.

In this paper we explore the use of soft actuation materials as active joints for propelling robotic fish, through combined analytical and computational modeling. In particular, we consider *short* beams of IPMC (or other soft actuation materials) that drive light, relatively rigid, passive links to enable underwater locomotion. Comparing to mechanisms based solely on movement of long IPMC beams, the proposed approach has several advantages: 1) with the link amplification effect, an active IPMC joint can produce large movement at the end of the link [16]; 2) it is more energy-efficient since the power consumption of an IPMC is approximately proportional to its surface area; and 3) the behavior of a short IPMC is less unpredictable and easier to control [17]. While the snake-like robot in [14] used IPMC to manipulate styrene foam links to produce undulatory body motion, long IPMCs were adopted. Furthermore, the work [14] was focused mainly on the prototype instead of its hydrodynamic modeling. On the other hand, although several groups have examined the modeling of underwater operation of IPMC [15], [18]–[21], little has been reported on the hydrodynamic modeling of multi-link manipulators with IPMC joints. Finally, soft actuation material-based active joints present a key challenge that is not critical for motor-actuated multi-link robotic fish or multi-link manipulators in general. In particular, the bending moment that an IPMC can produce depends highly on its internal dynamics and varies with its dimensions and frequencies. It is thus necessary to understand both the propulsion behavior and the required joint moments for various kinematic patterns. And this is the focus of our paper.

Both analytical modeling and computational fluid dynamics (CFD) modeling are pursued in this paper because of their complementary nature. With an assumption of inviscid flows, for given kinematic patterns of joints, analytical modeling provides the joint moments and thrust forces in explicit forms and allows efficient design analysis. CFD modeling, on the other hand, takes much longer computational time but it captures many nonlinear, complex effects (such as vortex shedding) that are ignored in analytical modeling. We also show that, from the computed joint moments, the required

This work was supported in part by US Civilian Research and Development Foundation (Grant# GUS16059), ONR (Grant# N000140810640, program manager Dr. T. McKenna), NSF (CAREER Grant# ECCS 0547131), Tartu University Foundation and Estonian Science Foundation (Grant #6765).

M. Anton is with the Smart Microsystems Laboratory, Department of Electrical and Computer Engineering, Michigan State University, East Lansing, MI 48824, USA, and with the IMS Lab, Institute of Technology, Tartu University, Nooruse 1, 50411 Tartu, Estonia. antonm@msu.edu

Z. Chen and X. Tan are with the Smart Microsystems Laboratory, Department of Electrical and Computer Engineering, Michigan State University, East Lansing, MI 48824, USA. chenzhe1@egr.msu.edu (Z. C.), xbtan@egr.msu.edu (X. T.)

M. Kruusmaa is with the Center for Biorobotics, Tallinn University of Technology, Akadeemia tee 15A, 12618 Tallinn, Estonia, and with the IMS Lab, Institute of Technology, Tartu University, Nooruse 1, 50411 Tartu, Estonia.

Send correspondence to X. Tan. Tel: 517-432-5671; Fax: 517-353-1980.

actuation voltages for the active joints can be computed using physics-based models for the soft actuation materials [22]; conversely, given the practical limitation on actuation voltages, we can derive the constraints (e.g., rotation magnitude at a given frequency) for the joints. The investigation is focused on a two-link tail attached to an anchored body since it captures the subtle features of multi-link fins with the least complexity (in both analysis and future prototype construction).

Computational results have shown that good agreement is achieved between the analytical modeling and the CFD modeling for different tail shapes and different kinematic patterns of joints. This points to a promising two-tier framework for the understanding and optimization of robotic fish with a multi-link tail. In particular, the analytical model will be instrumental in efficient, initial optimization over a large parameter space, and the result can then be used as a starting point for refined CFD optimization. Our studies have also shown that, comparing to a one-link bending tail, a two-link tail is able to produce much higher thrust and more versatile maneuvers, such as backward swimming.

The remainder of this paper is organized as follows. We present the analytical model in Section II. CFD modeling and the setup in FLUENT computation are discussed in Section III. In Section IV, we present the computational results, highlighting the comparison between the analytical and CFD approaches. We provide concluding remarks and comments for future work in Section V.

II. Analytical Modeling

Fig. 1 illustrates the configuration of robotic fish considered in this paper. The robot consists of a rigid body and a caudal fin (tail). The tail has two IPMC joints and two passive plates as links. The plates are assumed to be rigid but thin and light. In this paper the main body is assumed to be anchored and we focus on the thrust forces and joint moments developed via tail movement.

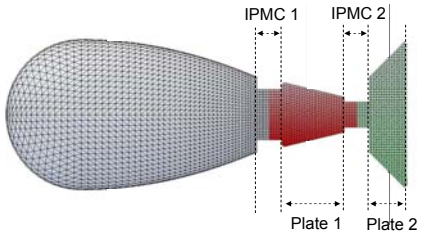

Fig. 1. Schematic of robotic fish with an IPMC-actuated, two-link tail.

A. Hydrodynamic Forces and Moments

The dimensions of the IPMC joints and passive links are defined as in Fig. 2. For $n=1,2$, α_n, ρ_n, and O_n denote the bending angle, curvature, and center location of the $n-$th IPMC joint. An inertial frame is defined through a set of orthonormal basis vectors $\{\vec{i},\vec{j},\vec{k}\}$, where $\vec{i}$ coincides with the longitudinal axis of the body, $\vec{j}$ is perpendicular to $\vec{i}$ and in the horizontal plane, while $\vec{k}$ is in the (upward) depth direction. As illustrated in Fig. 2, we also define, for $n=1,2$, $\vec{r}_n$ and $\vec{w}_n$ as unit vectors along and perpendicular to the $n-$th link, respectively. In terms of the reference frame, these vectors can be written as

$$\begin{aligned}
\vec{r}_1 &= \vec{i}\cos\alpha_1+\vec{j}\sin\alpha_1,\\
\vec{w}_1 &= -\vec{i}\sin\alpha_1+\vec{j}\cos\alpha_1,\\
\vec{r}_2 &= \vec{i}\cos(\alpha_1+\alpha_2)+\vec{j}\sin(\alpha_1+\alpha_2),\\
\vec{w}_2 &= -\vec{i}\sin(\alpha_1+\alpha_2)+\vec{j}\cos(\alpha_1+\alpha_2).
\end{aligned}$$

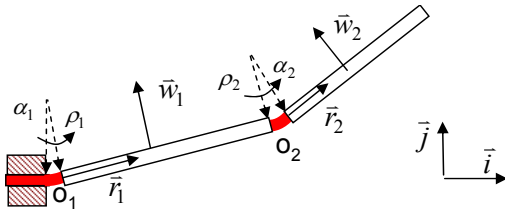

(a)

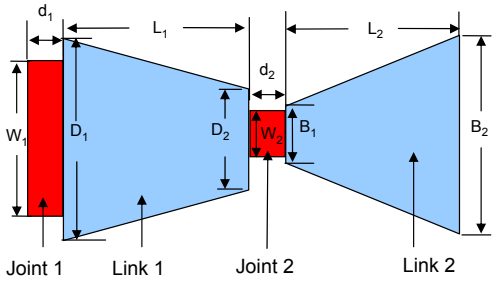

(b)

Fig. 2. Definition of variables for a two-link tail. (a) Top view; (b) side view.

We assume an inviscid, two-dimensional flow (in the $\vec{i}-\vec{j}$ plane). Since IPMCs are short and used as joints, we ignore the hydrodynamic forces due to IPMC movement. Given the joint angles $\alpha_1(t)$, $\alpha_2(t)$, we can derive the velocity of any point on Link 1 as

$$\vec{V}_1(\tau_1,t)=\tau_1\dot{\alpha}_1(t)\vec{w}_1,\ 0\le\tau_1<L_1, \tag{1}$$

and the velocity of any point on Link 2 as

$$\vec{V}_2(\tau_2,t)=\tau_2\dot{\alpha}_2(t)\vec{w}_2+L_1\dot{\alpha}_1(t)\vec{w}_1,\ 0\le\tau_2<L_2. \tag{2}$$

The hydrodynamic force acting on a moving rigid beam is proportional to the propelled virtual mass multiplied by the acceleration. The velocity of any point on a rigid link can be decomposed into two terms, $\vec{V}_\perp$ perpendicular to the link, and $\vec{V}_\parallel$ along the link. The assumption of inviscid flows implies that the virtual mass effect introduced by movement in the $\vec{V}_\parallel$ direction is negligible [23]. For Link 1, $\vec{V}_{1\perp}=\vec{V}_1$, and then the acceleration is

$$\vec{a}_{1\perp}(\tau_1,t)=\frac{d\vec{V}_1}{dt}=\tau_1\ddot{\alpha}_1(t)\vec{w}_1. \tag{3}$$

For Link 2, the velocity $\vec{V}_{2\perp}$ can be expressed as

$$\begin{aligned}
&\vec{V}_{2\perp}(\tau_2,t)=\left(\vec{V}_2\cdot\vec{w}_2\right)\vec{w}_2\\
=\ &\left(\tau_2\dot{\alpha}_2(t)+L_1\dot{\alpha}_1(t)\cos(\alpha_2(t))\right)\vec{w}_2,
\end{aligned}$$

where "·" represents the inner product of vectors. Then the acceleration is

$$\vec{a}_{2\perp}(\tau_2,t) = \frac{d\vec{V}_{2\perp}(\tau_2,t)}{dt} = (\tau_2\ddot{\alpha}_2(t) + \chi(t))\,\vec{w}_2, \quad (4)$$

where

$$\chi(t) = L_1(\ddot{\alpha}_1(t)\cos(\alpha_2(t)) - \dot{\alpha}_1(t)\,\dot{\alpha}_2(t)\sin(\alpha_2(t))). \quad (5)$$

The width of the links can be captured by

$$D(\tau_1) = D_1 - k_1\tau_1,\ 0 \le \tau_1 \le L_1, \quad (6)$$
$$B(\tau_2) = B_2 + k_2\tau_2,\ 0 \le \tau_2 \le L_2, \quad (7)$$

where $k_1 = \frac{D_1-D_2}{L_1}$, $k_2 = \frac{B_1-B_2}{L_2}$. The hydrodynamic force per unit length acting on the links are, for $\tau_1 \in [0, L_1]$, $\tau_2 \in [0, L_2]$,

$$\vec{F}_{\text{hydro1}}(\tau_1,t) = -\rho_w\frac{\pi}{4}D^2(\tau_1)\,\Gamma_1(\omega)\,\vec{a}_{1\perp}(\tau_1,t),$$
$$\vec{F}_{\text{hydro2}}(\tau_2,t) = -\rho_w\frac{\pi}{4}B^2(\tau_2)\,\Gamma_2(\omega)\,\vec{a}_{2\perp}(\tau_2,t),$$

where ρ_w is the density of fluid, and $\Gamma_n(\omega)$ is the hydrodynamic function for Link n, $n = 1, 2$. Note that $\Gamma_n(\omega)$ depends on the geometry and dimensions of the link and the frequency of the movement [24]. By integrating the hydrodynamic force density along each link and projecting it in the $-\vec{i}$ direction, we obtain the thrust forces on the two links:

$$T_1(t) = -\rho_w\frac{\pi}{4}\Gamma(\omega)\,\ddot{\alpha}_1(t)\,\lambda_f\sin(\alpha_1(t)),$$

$$T_2(t) = -\rho_w\frac{\pi}{4}\Gamma(\omega)\,(\ddot{\alpha}_2(t)\,\lambda_b + \lambda_c\chi(t))\sin(\alpha_1(t) + \alpha_2(t)),$$

The hydrodynamic force-induced bending moment on Joint 1 has two components, one from Link 1 and the other from Link 2:

$$M_1(t) = M_{11}(t) + M_{21}(t),$$

where

$$M_{11}(t) = \int_0^{L_1} \vec{r}_1\tau_1 \times \vec{F}_{\text{hydro1}}(\tau_1,t)\,d\tau_1,$$
$$M_{21}(t) = \int_0^{L_2} (\vec{r}_1 L_1 + \vec{r}_2\tau_2) \times \vec{F}_{\text{hydro2}}(\tau_2,t)\,d\tau_2.$$

The hydrodynamic force-induced bending moment on Joint 2 can be written as

$$M_2(t) = \int_0^{L_2} \vec{r}_2\tau_2 \times \vec{F}_{\text{hydro2}}(\tau_2,t)\,d\tau_2.$$

It can be derived that

$$M_1(t) = -\rho_w\frac{\pi}{4}\Gamma(\omega)\begin{pmatrix} \ddot{\alpha}_2(t)\,\lambda_a + \ddot{\alpha}_1(t)\,\lambda_e + \\ (L_1\cos(\alpha_2(t)) + \chi(t))\,\lambda_b \\ + L_1\cos(\alpha_2(t))\,\chi(t)\lambda_c \end{pmatrix},$$

$$M_2(t) = -\rho_w\frac{\pi}{4}\Gamma(\omega)\,(\ddot{\alpha}_2(t)\,\lambda_a + \chi(t)\lambda_b),$$

where

$$\lambda_a = \frac{B_1^2L_2^3}{3} + \frac{2k_2B_1L_2^4}{4} + \frac{k_2^2L_2^5}{5}, \quad (8)$$
$$\lambda_b = \frac{B_1^2L_2^2}{2} + \frac{2k_2B_1L_2^3}{3} + \frac{k_2^2L_2^4}{4}, \quad (9)$$
$$\lambda_c = B_1^2L_2 + \frac{2k_2B_1L_2^2}{2} + \frac{k_2^2L_2^3}{3}, \quad (10)$$
$$\lambda_e = \frac{D_1^2L_1^3}{3} - \frac{2k_1D_1L_1^4}{4} + \frac{k_1^2L_1^5}{5}, \quad (11)$$
$$\lambda_f = \frac{D_1^2L_1^2}{2} - \frac{2k_1D_1L_1^3}{3} + \frac{k_1^2L_1^4}{4}. \quad (12)$$

B. Incorporation of IPMC Dynamics

We can further incorporate the dynamics of the soft actuation materials into the analytical modeling framework to obtain the actuation voltages required to produce the given joint motions. Conversely, given the constraints on actuation voltages, this would enable us to compute the constraints on joint motions. In the IPMC case, the actuation-induced moments M_{a1} and M_{a2} satisfy, for $i = 1, 2$,

$$M_{ai}(t) = \frac{\rho_i(t)}{YI_i} - M_i(t), \quad (13)$$

where the curvature $\rho_i(t) = \alpha_i(t)/d_i$, Y is the effective Young's modulus of IPMC, $I_i = \frac{1}{12}W_ih^3$ is the area moment of inertia, h is the thickness of IPMC, and M_i is the hydrodynamic moment. A physics-based, control-oriented model for IPMC [22] can be used to relate the voltage input U_i to the actuation moment M_{ai} through an infinite-dimensional transfer function. Since IPMC joints are short, the effect of surface resistance can be ignored, which will simplify the model. The details are omitted here due to space limitation.

III. CFD Modeling

A. CFD Simulation Setup

FLUENT [25] is used in the CFD computation. The software computes the unsteady solution of the incompressible 3D Navier-Stokes equation under laminar flow conditions. Dynamic mesh update is adopted. A bounding box is defined to contain the robotic fish, while the fish itself defines another (moving) boundary for the fluid volume under consideration (Fig. 3). All boundary surfaces are defined as walls with zero slip conditions. An unstructured tetrahedral grid is used. For the anchored robotic fish simulated in this work, a bounding box ($21 \times 10 \times 10$ cm^3) is chosen, the volume grid of which has 15,172 nodes, 147,434 faces, and 70,245 cells. This has proven to be big enough to get accurate results on the forces acting on the tail. In particular, we have verified the independence of results from box size and grid density by doing simulations with a denser grid (33,794 nodes, 353,696 faces, and 171,691 cells) and a bigger bounding box ($31 \times 20 \times 20$ cm^3), and we have observed no notable changes in the computed forces or moments. In simulation, the robotic fish with a two-link tail is treated as three rigid links (with body counted as Link 0) connected with two joints. Each IPMC piece is divided in half and merged into

the adjacent links, with hinges assumed on its centerline. This is illustrated by the color scheme in Fig. 1.

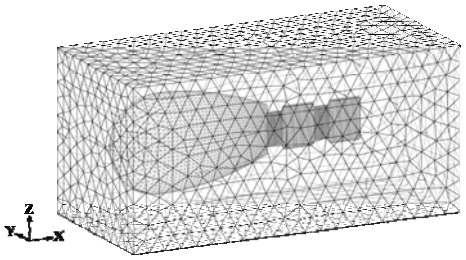

Fig. 3. Mesh of the bounding box containing the robotic fish.

B. Estimation of Forces and Moments

CFD simulation provides the distribution of pressure and viscous force density acting on each grid face. This information is used to compute the resulting thrust forces and joint moments, which will be further compared with the results from analytical modeling. Fig. 4 defines the variables used in force and moment analysis, while Fig. 5 shows the free-body diagram of the link i. Let C_i be the center of mass and center of inertia, and β_i be the link angle. Note $\beta_i = \beta_{i-1} + \alpha_i$, where α_i the joint angle. Let m_i and I_i be the mass and the moment of inertia, respectively. The hydrodynamic moment Q_i about C_i and the lumped hydrodynamic force G_i on the link are evaluated directly from the computed pressure and shear force distribution. We are interested in finding the moment M_i and the force F_i acting on the joint i. The latter also provides the information about the thrust forces on each link. In Fig. 5, the negative signs are introduced for M_{i+1} and F_{i+1} to indicate the reactive nature of joint force and moment for neighboring links.

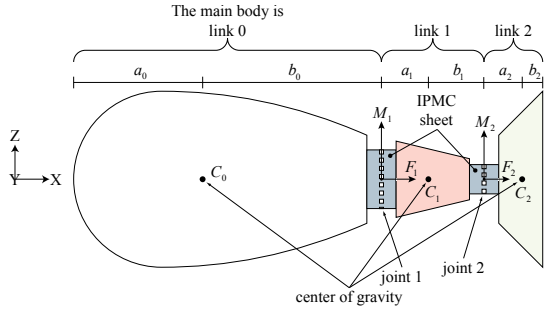

Fig. 4. Definition of variables for force and moment analysis.

The following force and moment balance equations are used to recursively evaluate F_i and M_i:

$$\begin{aligned} F_i &= F_{i+1} + m_i\ddot{X}_i - G_i, \\ M_i &= M_{i+1} + I_i\ddot{\beta}_i - Q_i + q(\beta_i)\times(a_iF_i + b_iF_{i+1}), \end{aligned} \quad (14)$$

where $q(\beta) = [\cos\beta \;\; \sin(\beta) \;\; 0]^T$, by using $F_N = 0$, $M_N = 0$ for the rightmost link N.

IV. Computational Results

A. Comparison between Analytical and CFD models

The kinematic patterns of joints take the following form:

$$\alpha_1(t) = A_1\sin(\omega_0 t), \;\; \alpha_2(t) = A_2\sin(\omega_0 t + \phi). \quad (15)$$

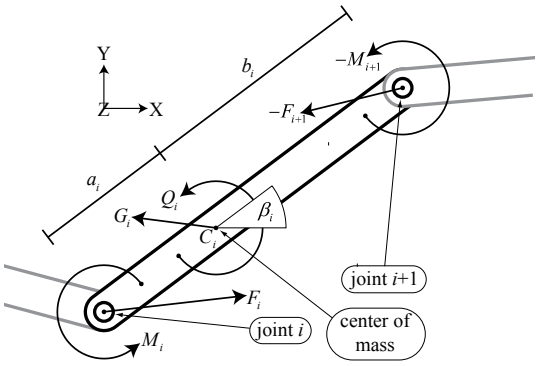

Fig. 5. Free-body diagram for the i-th link.

Three sets of kinematic patterns are used in the simulation, as listed in Table I. Pattern 1 and Pattern 2 differ in the phase delay, while Pattern 1 and Pattern 3 differ in joint amplitudes. We have chosen $\omega_0 = \pi$ rad/s throughout. The choice of the patterns used has otherwise been arbitrary.

TABLE I
KINEMATIC PATTERNS FOR JOINTS IN TWO-LINK TAIL.

Pattern #	$A_1(^\circ)$	$A_2(^\circ)$	$\phi(^\circ)$
1	10	15	90
2	10	15	60
3	19	28.5	90

The dimensions of the tail (refer to Fig. 2(b)) are: $B_1 =$ 3 cm, $B_2 = 6$ cm, $D_1 = 2.6$ cm, $D_2 = 1.6$ cm, $d_1 = d_2 =$ 1 cm, $W_1 = 2$ cm, $W_2 = 1$ cm, $L_1 = 2.5$ cm, $L_2 = 1.5$ cm. The hydrodynamic function $\Gamma_1 = 1.11 + 1.53j$ for Joint 1 and $\Gamma_2 = 1$ for Joint 2. The thrust forces computed for the three joint patterns are presented in Figs. 6−8. Despite minor discrepancies, the comparison between the analytical model and the CFD model is generally good, supporting the validity of the analytical model in the tested range. A good match is also achieved for the prediction of joint moments, but those results are omitted here due to the space constraint. Comparing Fig. 6 and Fig. 7, we can clearly see the impact of phase delay ϕ on the propulsion performance: a 50% increase of thrust is obtained when ϕ is changed from 90° to 60°. Another interesting observation is that, for all three patterns of joint angles, the thrust from Link 2 is much bigger than that from Link 1.

Using the approach discussed in Section II-B, we have also calculated the voltage inputs to the IPMC joints for generating the given joint angles. Parameters for the IPMC model follow that identified in [22]. The results shown that, while Patterns #1 and #2 can be delivered with actuation voltages under 3 V, Pattern #3 requires over 5 V on Joint 2, which exceeds the typical recommended range for IPMC actuators.

B. Comparison with One-link Tail

We further compare the two-link tail with a one-link tail, which is illustrated in Fig. 9. The dimensions of the link are the same as those of Link 2 for the two-link tail, while the dimensions of the IPMC joint are the same as those of Joint 1 for the two-link tail. For the joint pattern

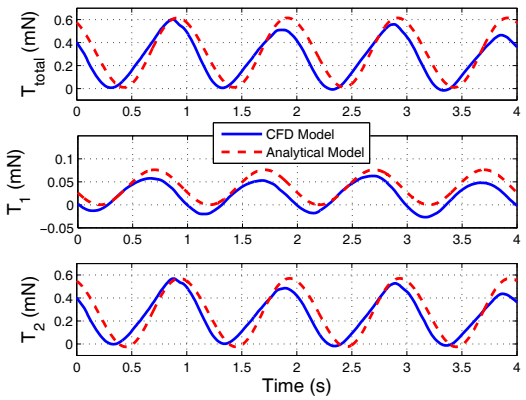

Fig. 6. Thrust forces for a two-link tail (Pattern #1).

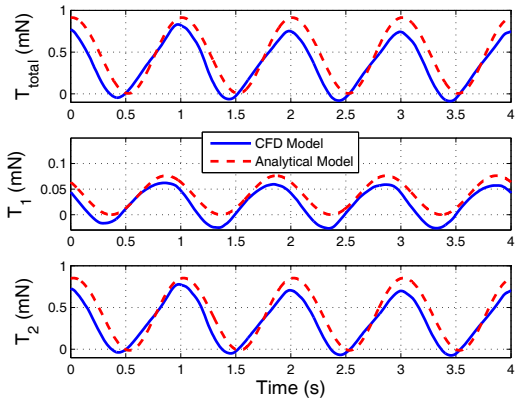

Fig. 7. Thrust forces for a two-link tail (Pattern #2).

$\alpha(t) = A\sin(\omega_0 t)$ with $A = 10°$, the thrust force from the one-link tail is about 5% of that from the two-link tail under Pattern #2 (Fig. 10). This translates to the result that, with approximately four times of power consumption, the robot with two-link tail could achieve about 90 times of useful propulsion power comparing to the robot with one-link tail. In other words, significant enhancement of power efficiency could be achieved with the robot that has a two-link tail.

C. Backward Thrust

While a robotic fish with a one-link tail can only achieve forward motion, we show that, under proper amplitude and phase conditions, the robot with two-link tail could achieve backward swimming, a useful maneuver for underwater robots. Fig. 11 shows the CFD results for the two-link tail with trapezoidal links, where both joint angles have large amplitudes, $A_1 = 20°$, $A_2 = 50°$, and the second joint leads the first by 150°. The kinematic actuation pattern was found via trial and error. The total thrust is predominantly negative, with the major contribution from Link 2. Fig. 12 further shows the velocity field in this case, where the region of highest flow velocities seems to be concentrated between the two links. In the case of predominantly positive thrust, however, the flow velocities (not shown in this paper) seem to be largest around the second link and in the immediate wakes. We note that the analytical model fails to produce a predominantly negative thrust. This is likely due to that the

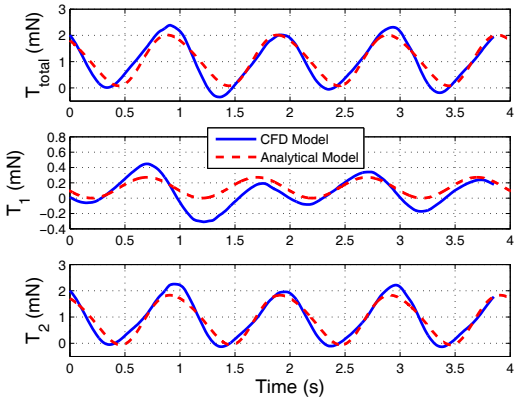

Fig. 8. Thrust forces for a two-link tail (Pattern #3).

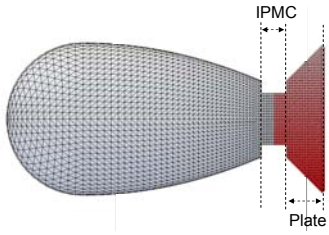

Fig. 9. Illustration of robotic fish with one-link tail.

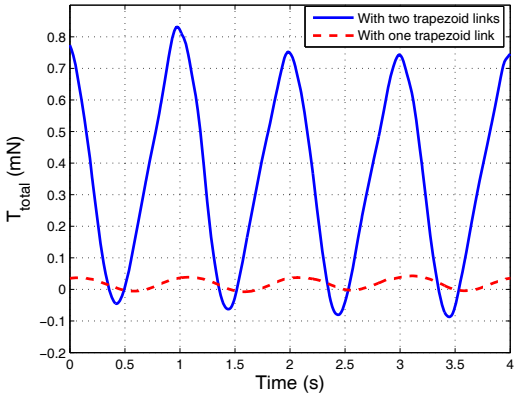

Fig. 10. Thrust forces for a two-link tail and a one-link tail (CFD results).

negative thrust arises from interactions of vortices induced by the two links, and such effects are not captured by the analytical model.

V. Conclusion and Future Work

In this paper we have presented a joint analytical and CFD modeling study of robotic fish propelled by a multi-link tail actuated by soft materials-enabled active joints. Extensive computational results have shown that the analytical model is able to predict the thrust force and the hydrodynamic moments on the joints for a range of kinematic patterns. On the other hand, some discrepancies exist between the predictions from the analytical model and the CFD results, especially for large-amplitude joint motions. This is because the (much more computationally expensive) CFD calculation is able to capture subtle effects, such as three-dimensional flows and vortex shedding. Therefore, our results suggest a promising two-tier approach to the modeling and optimiza-

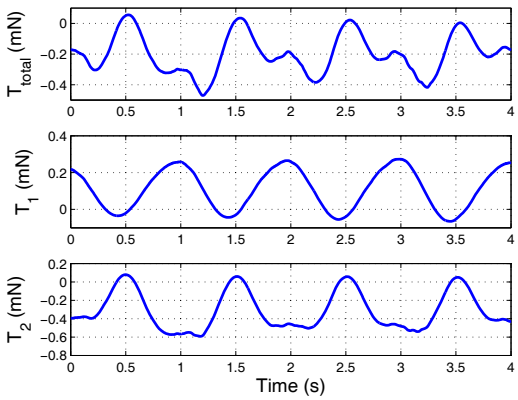

Fig. 11. Predominantly negative thrust for a two-link tail (CFD results).

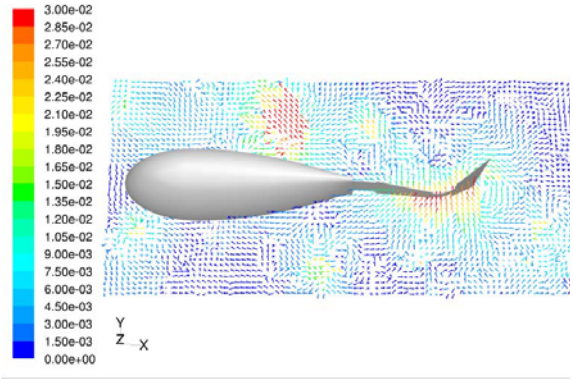

Fig. 12. Velocity field for predominantly backward thrust.

tion of robotic fish with a multi-link tail: using the analytical model for rapid but coarse search of the parameter space, and using the CFD for refined search and optimization. The presented modeling framework also allows us to derive the operational constraints of the active joints by incorporating the internal dynamics of actuation materials.

The kinematic gaits used in this paper have been chosen somewhat arbitrarily. In future work we will use the proposed modeling approach to optimize the design of both the robot and the gaits, in order to achieve excellent thrust output and energy efficiency. we will also extend the study to the case of a free-swimming robot. The connection between a two-link tail and a pitching and heaving plate will be explored. Finally, the development of a robotic fish prototype is underway, which will be used to validate the findings from the analytical and CFD modeling effort.

REFERENCES

[1] F. E. Fish and G. V. Lauder, "Passive and active flow control by swimming fishes and mammals," *Annual Review of Fluid Mechanics*, vol. 38, pp. 193–224, 2006.

[2] M. S. Triantafyllou and G. S. Triantafyllou, "An efficient swimming machine," *Scientific America*, vol. 273, no. 3, pp. 64–70, 1995.

[3] S. Guo, T. Fukuda, and K. Asaka, "A new type of fish-like underwater microrobot," *IEEE/ASME Transactions on Mechatronics*, vol. 8, no. 1, pp. 136–141, 2003.

[4] H. Hu, J. Liu, I. Dukes, and G. Francis, "Design of 3D swim patterns for autonomous robotic fish," in *Proceedings of the 2006 IEEE/RSJ International Conference on Intelligent Robots and Systems*, Beijing, China, 2006, pp. 2406–2411.

[5] B. Kim, D. Kim, J. Jung, and J. Park, "A biomimetic undulatory tadpole robot using ionic polymer-metal composite actuators," *Smart Materials and Structures*, vol. 14, pp. 1579–1585, 2005.

[6] X. Tan, D. Kim, N. Usher, D. Laboy, J. Jackson, A. Kapetanovic, J. Rapai, B. Sabadus, and X. Zhou, "An autonomous robotic fish for mobile sensing," in *Proceedings of the IEEE/RSJ International Conference on Intelligent Robots and Systems*, Beijing, China, 2006, pp. 5424–5429.

[7] K. A. Morgansen, B. I. Triplett, and D. J. Klein, "Geometric methods for modeling and control of free-swimming fin-actuated underwater vehicles," *IEEE Transactions on Robotics*, vol. 23, no. 6, pp. 1184–1199, 2007.

[8] J. W. Paquette and K. J. Kim, "Ionomeric electroactive polymer artificial muscle for naval applications," *IEEE Journal of Oceanic Engineering*, vol. 29, no. 3, pp. 729–738, 2004.

[9] D. Trivedi, C. D. Rahn, W. M. Kier, and I. D. Walker, "Soft robotics: Biological inspiration, state of the art, and future research," *Applied Bionics and Biomechanics*, vol. 5, no. 3, pp. 99–117, 2008.

[10] J. Tangorra, P. Anquetil, T. Fofonoff, A. Chen, M. Del Zio, and I. Hunter, "The application of conducting polymers to a biorobotic fin propulsor," *Bioinspiration & Biomimetics*, vol. 2, pp. S6–S17, 2007.

[11] S. McGovern, G. Alici, V. T. Truong, and G. Spinks, "Finding NEMO (Novel Electromaterial Muscle Oscillator): A polypyrrole powered robotic fish with real-time wireless speed and directional control," *Smart Material and Structures*, vol. 18, p. 095 009:1C10, 2009.

[12] M. Mojarrad and M. Shahinpoor, "Biomimetic robotic propulsion using polymeric artificial muscles," in *Proceedings of the IEEE International Conference on Robotics and Automation*, Albuquerque, NM, 1997, pp. 2152–2157.

[13] A. Punning, M. Anton, M. Kruusmaa, and A. Aabloo, "A biologically inspired ray-like underwater robot with electroactive polymer pectoral fins," in *Proceedings of the 2004 IEEE International Conference on Mechatronics and Robotics*, Aachen, Germany, 2004, pp. 241–245.

[14] N. Kamamichi, M. Yamakita, K. Asaka, and Z. Luo, "A snake-like swimming robot using IPMC actuator/sensor," in *Proceedings of the 2006 IEEE International Conference on Robotics and Automation*, Orlando, FL, 2006, pp. 1812–1817.

[15] E. Mbemmo, Z. Chen, S. Shatara, and X. Tan, "Modeling of biomimetic robotic fish propelled by an ionic polymer-metal composite actuator," in *Proceedings of the IEEE International Conference on Robotics and Automation*, 2008, pp. 689–694.

[16] I. Must, M. Anton, M. Kruusmaa, and A. Aabloo, "Linear modeling of elongated bending EAP actuator at large deformations," in *Electroactive Polymer Actuators and Devices (EAPAD) XI, Proceedings of SPIE*, Y. Bar-Cohen, Ed., 2009, p. 728723.

[17] A. Hunt, A. Punning, M. Anton, A. Aabloo, and M. Kruusmaa, "A multilink manipulator with IPMC joints," in *Electroactive Polymer Actuators and Devices (EAPAD) 2008, Proceedings of SPIE*, Y. Bar-Cohen, Ed., vol. 6927, 2008, p. 69271Z.

[18] K. J. Kim, W. Yim, J. W. Paquette, and D. Kim, "Ionic polymer-metal composites for underwater operation," *Journal of Intelligent Material Systems and Structures*, vol. 18, pp. 123–132, 2007.

[19] Z. Chen, S. Shatara, and X. Tan, "Modeling of biomimetic robotic fish propelled by an ionic polymer-metal composite caudal fin," *IEEE/ASME Transactions on Mechatronics*, 2009, to appear.

[20] P. Brunetto, L. Fortuna, S. Graziani, and S. Strazzeri, "A model of ionic polymercmetal composite actuators in underwater operations," *Smart Material and Structures*, vol. 17, pp. 025 029:1–12, 2008.

[21] K. Abdelnour, E. Mancia, S. D. Peterson, and M. Porfiri, "Hydrodynamics of underwater propulsors based on ionic polymer metal composites: A numerical study," *Smart Material and Structures*, vol. 18, p. 085 006:1C11, 2009.

[22] Z. Chen and X. Tan, "A control-oriented and physics-based model for ionic polymer-metal composte actuators," *IEEE/ASME Transactions on Mechatronics*, vol. 13, no. 5, pp. 519–529, 2008.

[23] M. J. Lighthill, "Large-amplitude elongated-body theory of fish locomotion," *Proceedings of the Royal Society of London B*, vol. 179, pp. 125–138, 1971.

[24] J. E. Sader, "Frequency response of cantilever beams immersed in viscous fluids with applications to the atomic force micrscope," *Journal of Applied Physics*, vol. 84, no. 1, pp. 64–76, 1998.

[25] http:\\www.fluent.com.